

Support information

Highly reversible and long-life aqueous zinc-ion battery based on ultrathin (NH₄)₂V₁₀O₂₅·8H₂O nanobelts

Tongye Wei¹, Qian Li¹, Gongzheng Yang^{1*}, Chengxin Wang^{1,2*}

*¹State Key Laboratory of Optoelectronic Materials and Technologies, School of
Physics Science and Engineering, Sun Yat-sen (Zhongshan) University, Guangzhou
510275, People's Republic of China*

*²The Key Laboratory of Low-carbon Chemistry & Energy Conservation of
Guangdong Province, Sun Yat-sen (Zhongshan) University, Guangzhou 510275,
People's Republic of China*

*Correspondence and requests for materials should be addressed to C. X. Wang & G.
Z. Yang.

Tel & Fax: +86-20-84113901

E-mail: wchengx@mail.sysu.edu.cn; ygongzh@mail2.sysu.edu.cn

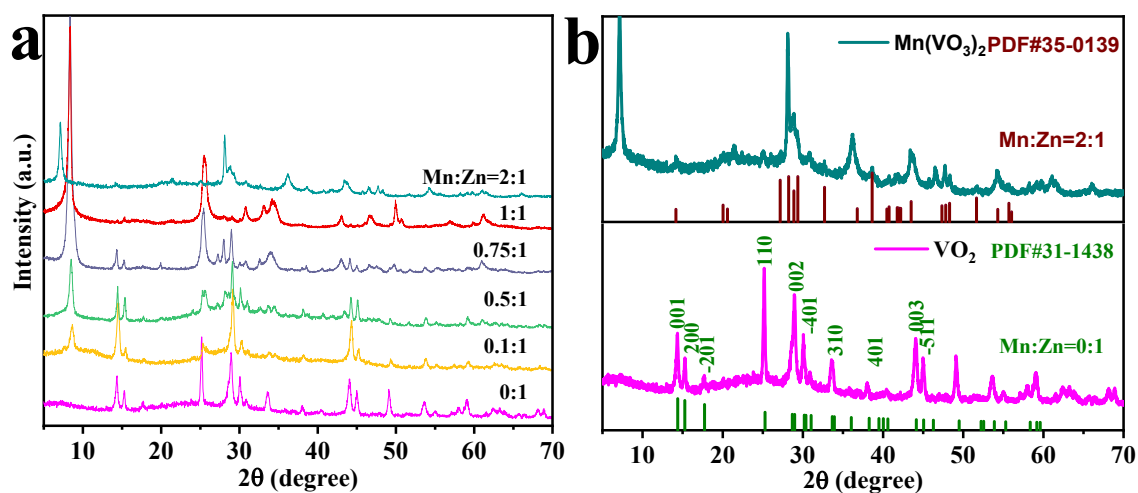


Figure S1 a) XRD patterns of the prepared materials with adding different amount of MnSO₄, b) the detail XRD patterns of Mn(VO₃)₂ and VO₂.

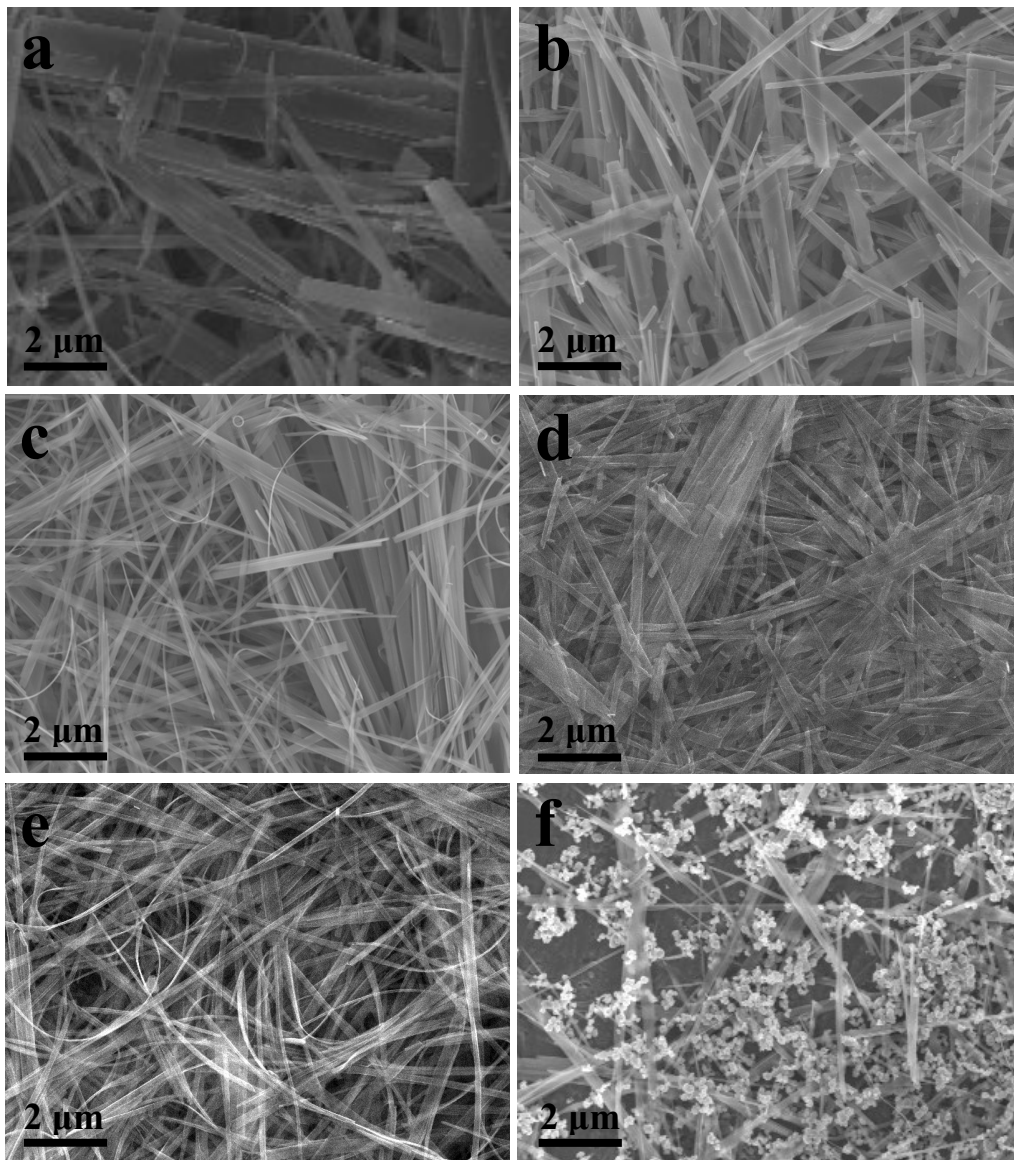


Figure S2 SEM images of the prepared materials with adding different amount of MnSO_4 , a) Mn:V=0:1, b) Mn:V=0.1:1, c) Mn:V=0.5:1, d) Mn:V=0.75:1, e) Mn:V=1:1, and f) Mn:V=2:1.

The formation mechanism of 1D vanadium-based oxide is usually attributed to the well-known “Ostwald ripening mechanism”, which has been widely studied by Chen *et al.* and many other researchers.^{1,2} To investigate the role of $\text{MnSO}_4 \cdot \text{H}_2\text{O}$ in the formation of the ultrathin $(\text{NH}_4)_2\text{V}_{10}\text{O}_{25} \cdot 8\text{H}_2\text{O}$ nanobelts, the samples obtained at different experimental conditions by adjusting the contents of $\text{MnSO}_4 \cdot \text{H}_2\text{O}$ were carefully characterized. Figure S1a shows the XRD patterns of the synthesized samples. The XRD pattern of the sample prepared without adding $\text{MnSO}_4 \cdot \text{H}_2\text{O}$ can be indexed to monoclinic VO_2 with lattice constants: $a=1.20$, $b=0.37$, $c=0.64$ nm, and $\beta=106.6^\circ$ (JCPDS 31-1438). The peak at $\sim 10.4^\circ$ appeared as adding a small amount of $\text{MnSO}_4 \cdot \text{H}_2\text{O}$ (Mn:V mole ratio 0.1:1) and shifted to a lower degree, indicating that the lattice constant become large with increasing the $\text{MnSO}_4 \cdot \text{H}_2\text{O}$ concentration. In addition, the peaks at $\sim 28.9^\circ$, 30.1° , 44.1° , 45.2° , 49.5° , which belong to VO_2 , gradually disappear with continuous adding $\text{MnSO}_4 \cdot \text{H}_2\text{O}$. When the Mn:V ratio is set to 2:1, the XRD pattern can be assigned to $\text{Mn}(\text{VO}_3)_2$ (JCPDS 35-0139). As shown in the Figure S2 the SEM demonstrate the nanobelts were become thinner with increasing content of $\text{MnSO}_4 \cdot \text{H}_2\text{O}$, until the Mn:V ratio is 2:1 the material is composed of nanobelts and nanoparticle.”

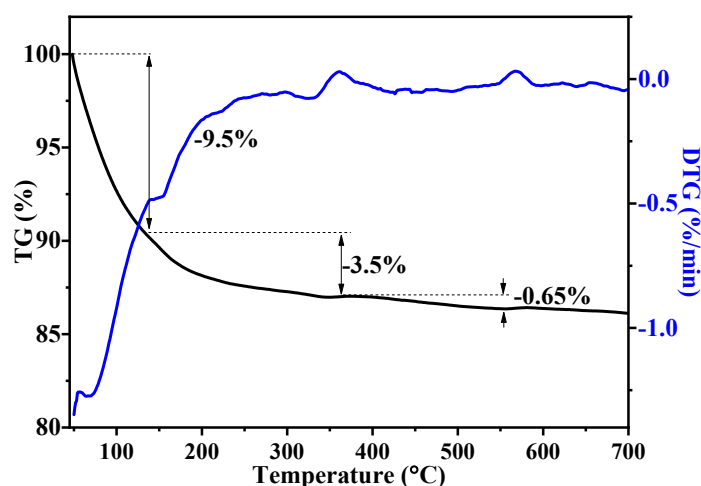


Figure S3. TG result of the $V_{10}O_{24} \cdot 12H_2O$ obtained from room temperature to 700 °C in air atmosphere at heating rate of 10 °C min⁻¹. To investigate the water content, thermogravimetry (TG) was conducted and the plot is shown in Figure R3. In accordance with literature data, (Adv. Energy Mater., 2017, 7, 1602720) the temperature increases from room temperature to 150 °C, the weight loss is generally attributed to the physically absorbed water. More strongly bound water (structural water) departs between 150 °C and 350 °C. When heated to 350 °C, complete removal of water (~12.8%) was found, corresponding to 7.6 moles of H₂O per mole of (NH₄)₂V₁₀O₂₅. However, by considering the weight loss from 150 °C to 350 °C, we estimate that there are 2.05 moles of structural water molecules in each formula unit of (NH₄)₂V₁₀O₂₅. In brief, the estimated H₂O content is less than 8, which cause the impurity phase as mentioned in the question 2. Besides, the weight loss between 350 °C and 650 °C may because of the release of ammonia and the oxidation of vanadium element.

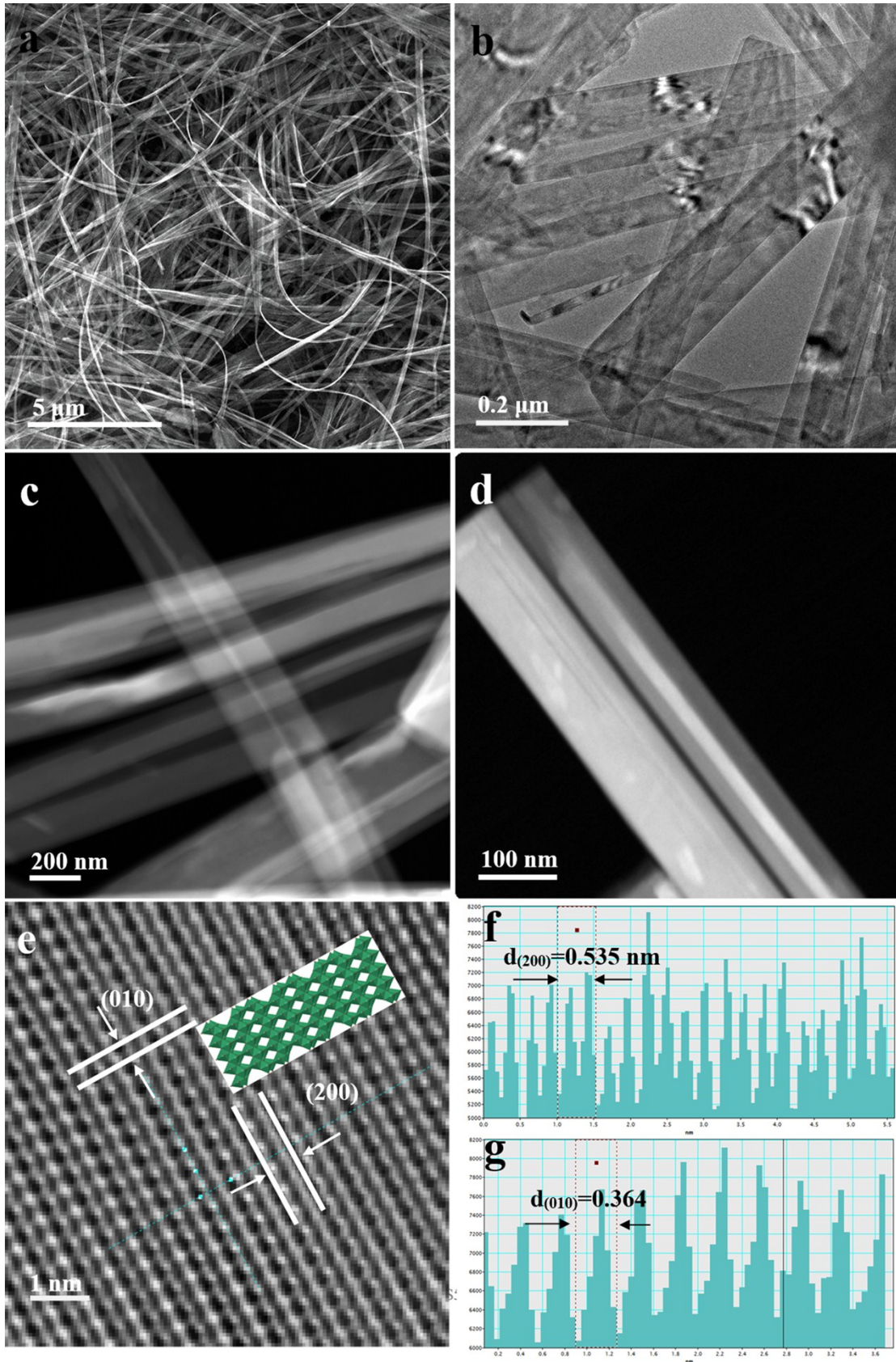


Figure S4 a) A SEM image of the $(\text{NH}_4)_2\text{V}_{10}\text{O}_{25}\cdot 8\text{H}_2\text{O}$ nanobelts. b) A panoramic TEM image of the nanobelts. c and d) STEM of the prepared $(\text{NH}_4)_2\text{V}_{10}\text{O}_{25}\cdot 8\text{H}_2\text{O}$ nanobelts. e) A HRTEM image of an individual nanobelt with high crystallinity. f) The (200) lattice fringes with a d-spacing of 0.535 nm and the (010) lattice fringes with a d-spacing of 0.364 nm.

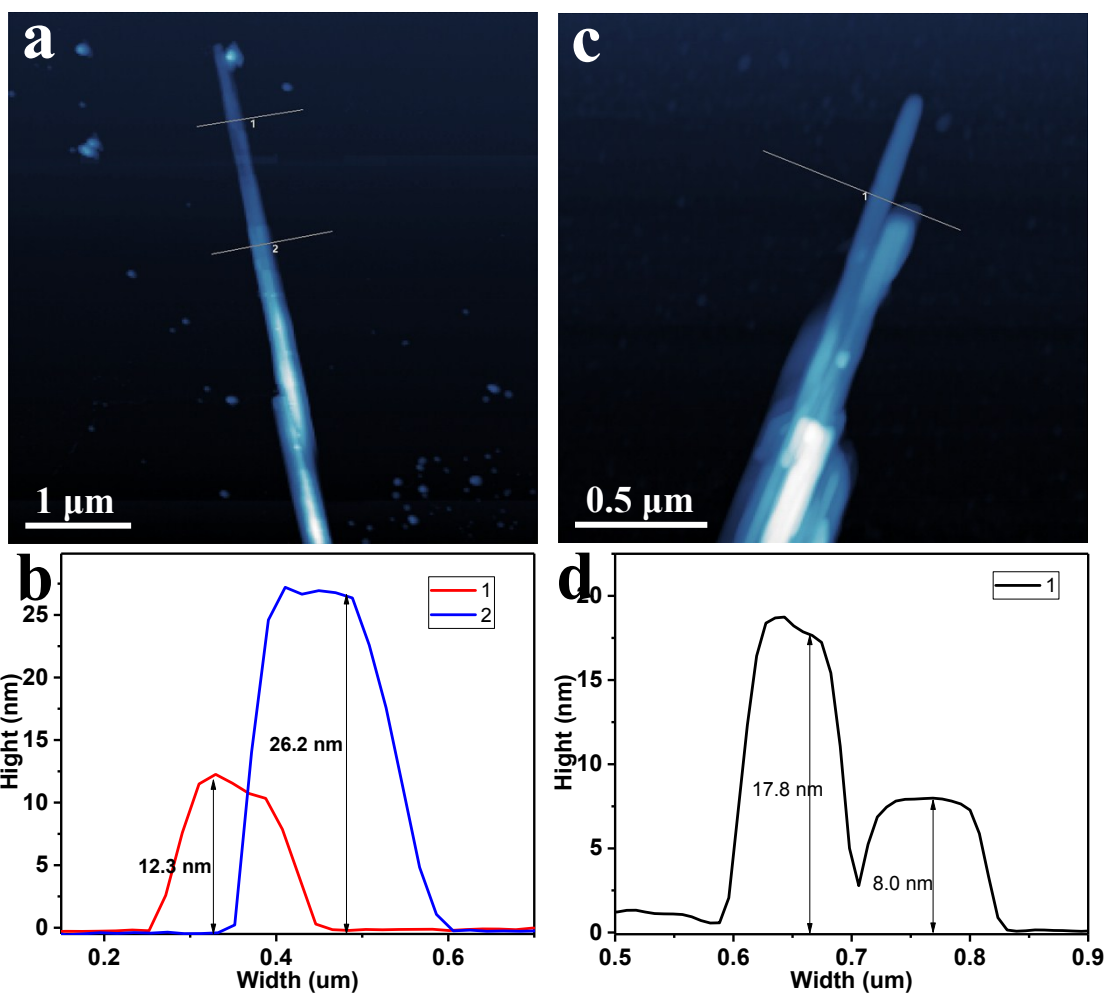


Figure S5 a, c) AFM images of single nanobelts. b, d) Cross-sectional profile shows the thickness of the single layer nanobelts is around 10 nm.

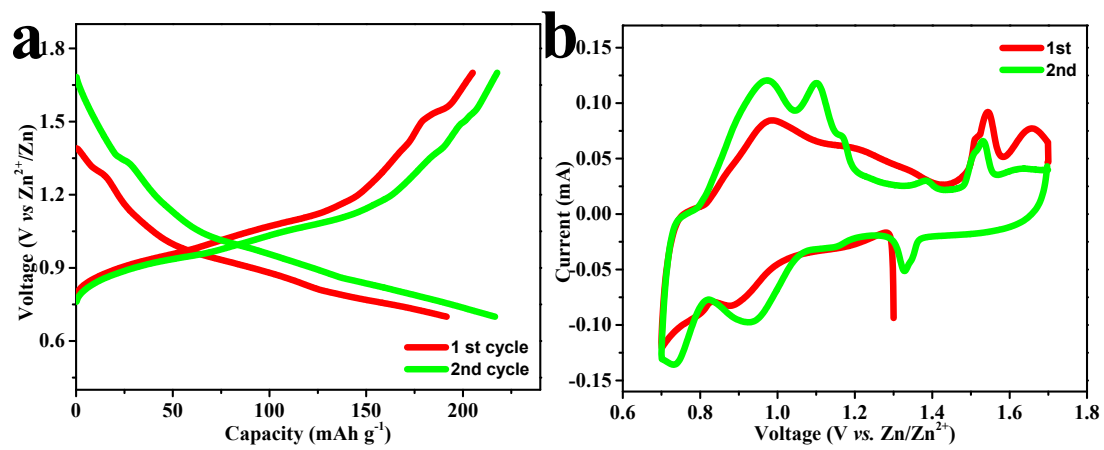


Figure S6 a) Discharge-Charge and b) CV curves of $(\text{NH}_4)_2\text{V}_{10}\text{O}_{25}\cdot 8\text{H}_2\text{O}$ -based electrodes prepared in the first two cycles.

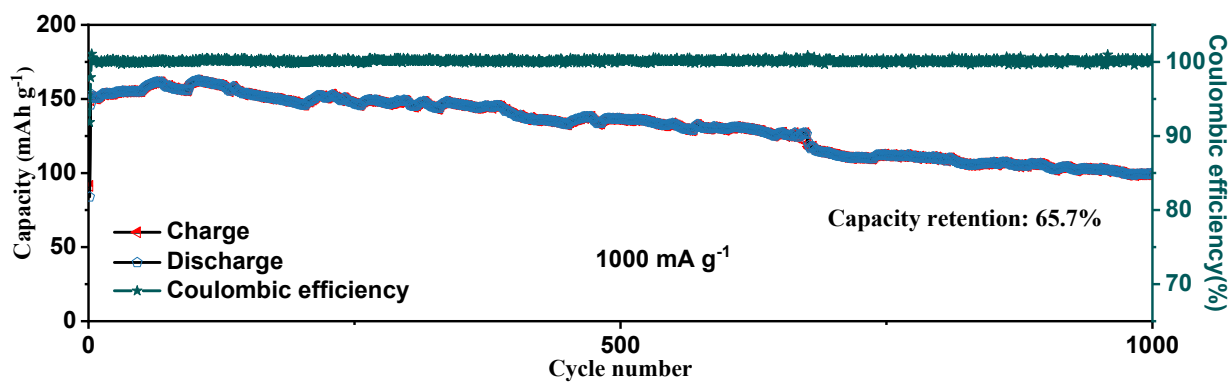


Figure S7. Cycling performances of the $(\text{NH}_4)_2\text{V}_{10}\text{O}_{25}\cdot 8\text{H}_2\text{O}$ /Zn Cell using 2M ZnSO_4 aqueous electrolyte. The capacity retention of 65.7% after 1000 cycles is unsatisfied by compared with 91.2% using 3 M $\text{Zn}(\text{CF}_3\text{SO}_3)_2$ electrolyte.

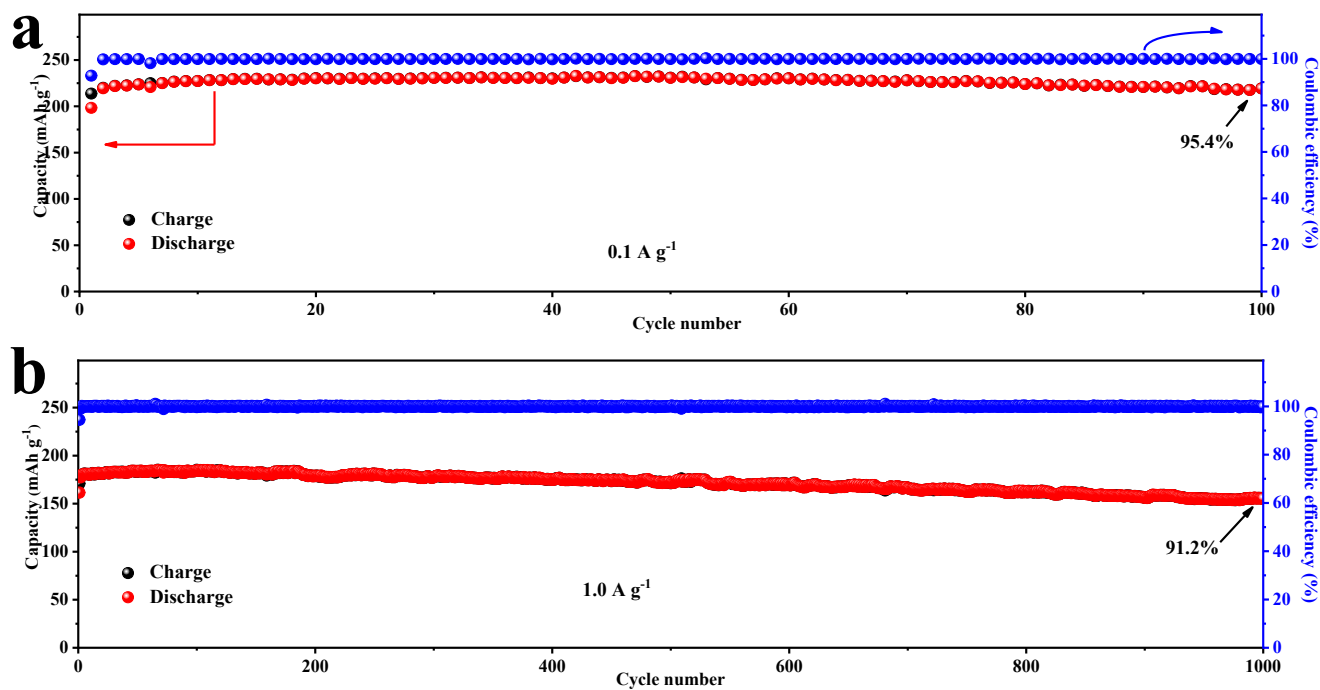


Figure S8. Cycling performances of the $(\text{NH}_4)_2\text{V}_{10}\text{O}_{25}\cdot 8\text{H}_2\text{O} / \text{Zn}$ Cell. Capacity as a function of cycle number obtained at the current densities of a) 0.1, and b) 1 A g^{-1} .

GITT measurement

The GITT test, consisting of a series of current pulses ($\approx 50 \text{ mA g}^{-1}$) for 10 min followed by a 1 h relaxation process, was performed using the Neware battery testing system with 0.7 and 1.7 V (vs Zn^{2+}/Zn) as the low and high cutoff voltages. The chemical diffusion coefficient $D_{\text{Zn}^{2+}}$ in the active material can be estimated according to the following equation:

$$D_{\text{Zn}^{2+}} = (4/\pi\tau) * [n_M V_M/S]^2 [\Delta E_S/\Delta E_t]^2$$

where, τ is the constant current pulse duration; n_M and V_M are the moles and molar volume of $(\text{NH}_4)_2\text{V}_{10}\text{O}_{25}\cdot 8\text{H}_2\text{O}$, respectively; S is the electrode-electrolyte interface area (taken as the geometric area of the electrode $\sim 1.131\text{cm}^2$); ΔE_S , and ΔE_t are the change in the steady state voltage and overall cell voltage after the application of a current pulse in a single step GITT experiment, respectively.^{3,4}

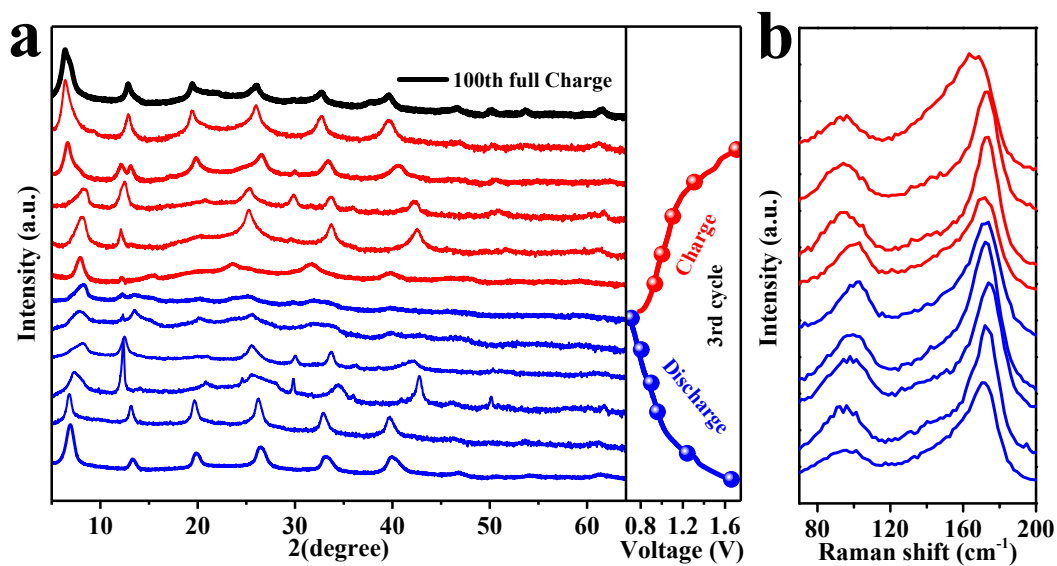


Figure S9 a) XRD patterns of $(\text{NH}_4)_2\text{V}_{10}\text{O}_{25}\cdot 8\text{H}_2\text{O}$ electrodes collected at various states of the third cycles. b) The detail Raman spectral of $(\text{NH}_4)_2\text{V}_{10}\text{O}_{25}\cdot 8\text{H}_2\text{O}$ electrodes during charging and discharging progress of the second cycle.

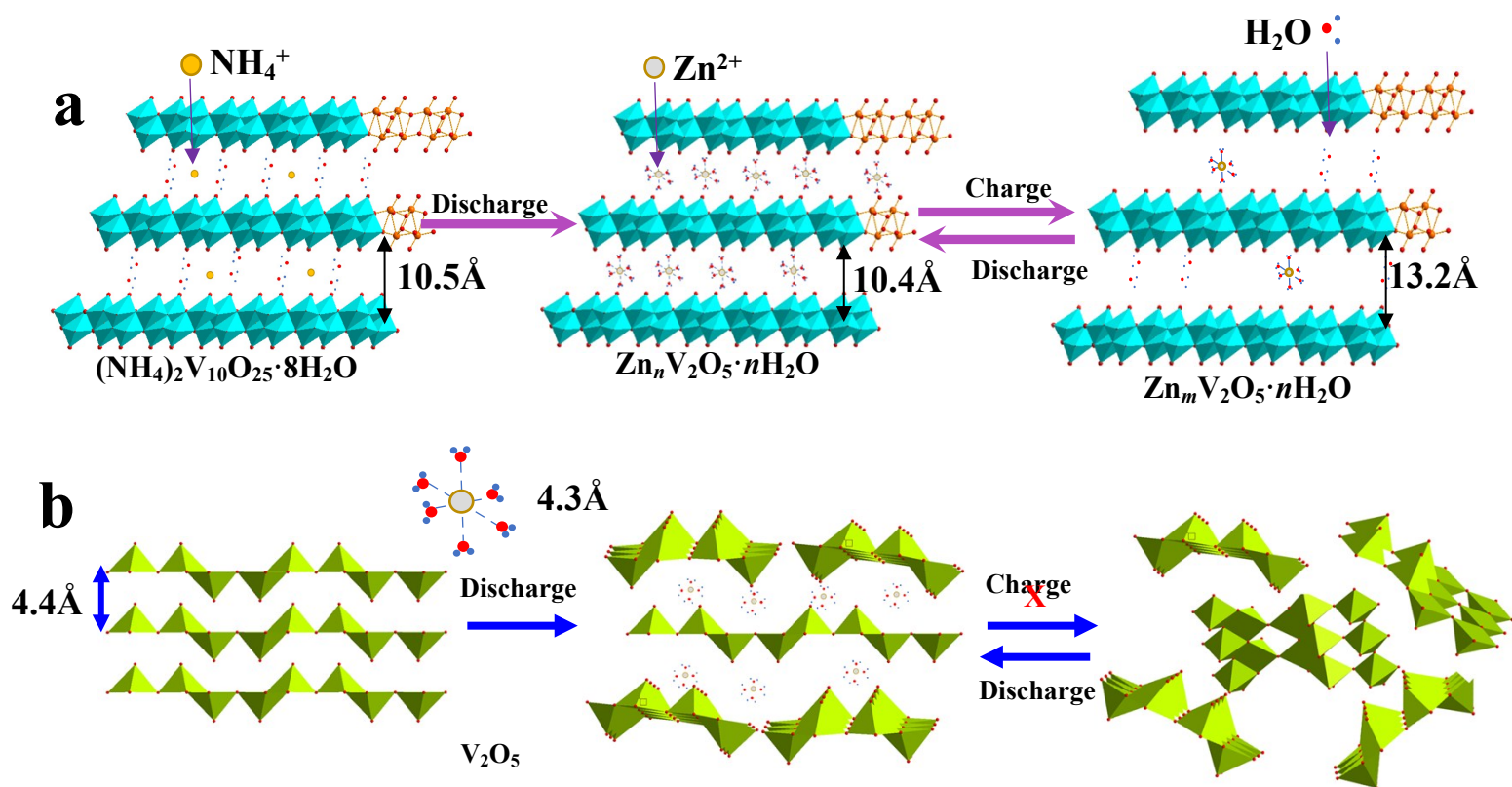


Figure S10 a) The potential structure evolution of the prepared $(\text{NH}_4)_2\text{V}_{10}\text{O}_{25}\cdot 8\text{H}_2\text{O}$ during Zn insertion/extraction. The $(\text{NH}_4)_2\text{V}_{10}\text{O}_{25}\cdot 8\text{H}_2\text{O}$ displays an interlayer spacing of 10.45 Å, which is similar to the hydrated vanadium pentoxide ($\text{V}_2\text{O}_5\cdot n\text{H}_2\text{O}$). The structure composition of bilayered which are more stable, the interlamellar spacing between the bilayered was connected by the so-called electrostatic attraction which was adjustable from 10.45 to 13.2 Å along with the Zn^{2+} insertion/de-insertion.^{3, 5}

b) Orthorhombic V_2O_5 ($\alpha\text{-V}_2\text{O}_5$) with interlayer spacing of 4.4 Å is not suitable for long-term reversible $\text{Zn}(\text{H}_2\text{O})^{2+}$ ion (radius of 4.3 Å) insertion/extraction, since the layered structure will be flaking which leads to capacity fading after the first cycle.⁶

Table S1. The main elements content of the pristine $(\text{NH}_4)_2\text{V}_{10}\text{O}_{25}\cdot 8\text{H}_2\text{O}$ and the $(\text{NH}_4)_2\text{V}_{10}\text{O}_{25}\cdot 8\text{H}_2\text{O}$ electrodes collected at fully discharge/charge states in the first two cycles

Samples	XPS				
	V (at.%)	O (at.%)	Zn (at.%)	Mn (at.%)	N (at.%)
pristine	24.42	69.4	-	1.48	4.67
1 st discharge	21.04	65.57	13.13	-	-
1 st charged	23.09	72.74	3.99	-	-
2 nd discharged	20.88	65.39	13.42	-	-
2 nd charge	22.03	72.14	5.62	-	-

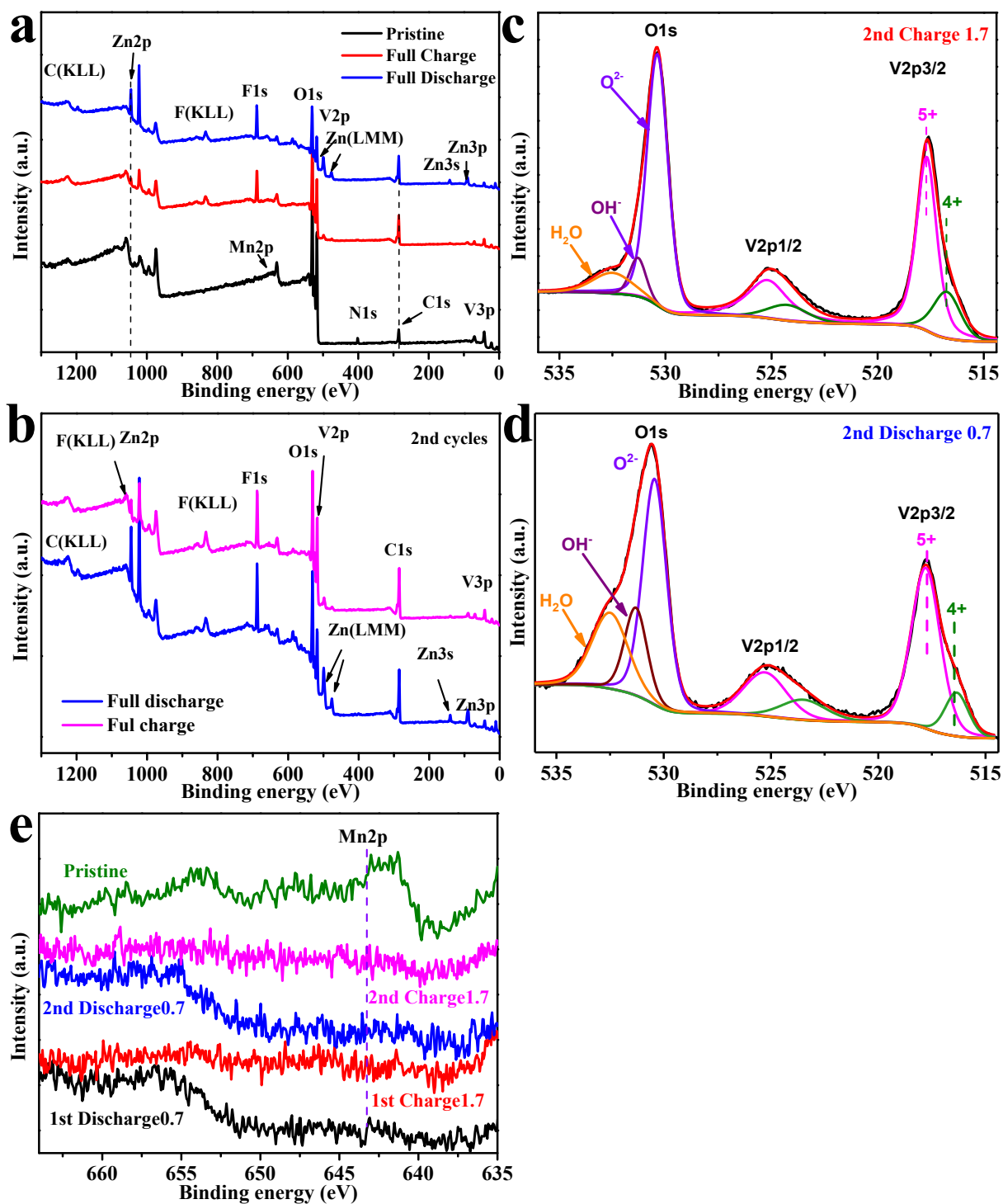


Figure S11 XPS spectra of the $(\text{NH}_4)_2\text{V}_{10}\text{O}_{25}\cdot 8\text{H}_2\text{O}$ electrodes. a, b) Survey spectra, c, d) V 2p and O 1s region of the XPS spectra in the second cycle. e) Mn 2p region obtained at first two cycles and the pristine $(\text{NH}_4)_2\text{V}_{10}\text{O}_{25}\cdot 8\text{H}_2\text{O}$.

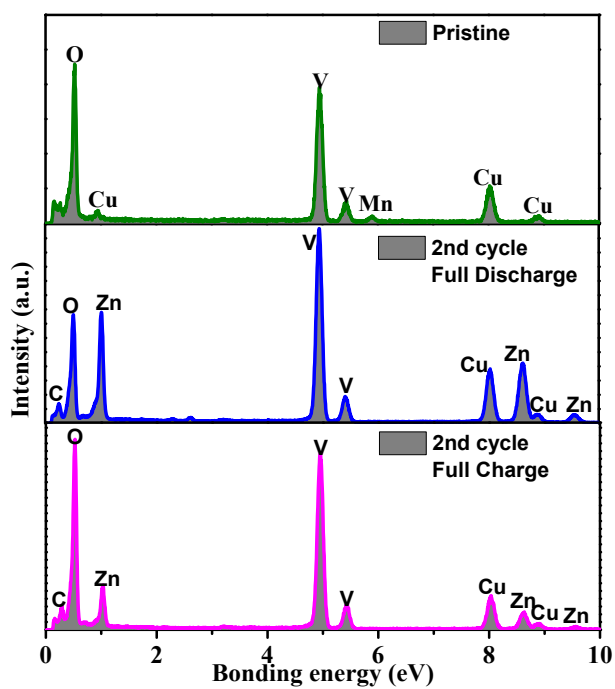


Figure S12 Energy dispersive X-ray spectra of the $(\text{NH}_4)_2\text{V}_{10}\text{O}_{25}\cdot 8\text{H}_2\text{O}$ electrodes collected at fully discharge/charge states in the second cycle and the pristine $(\text{NH}_4)_2\text{V}_{10}\text{O}_{25}\cdot 8\text{H}_2\text{O}$.

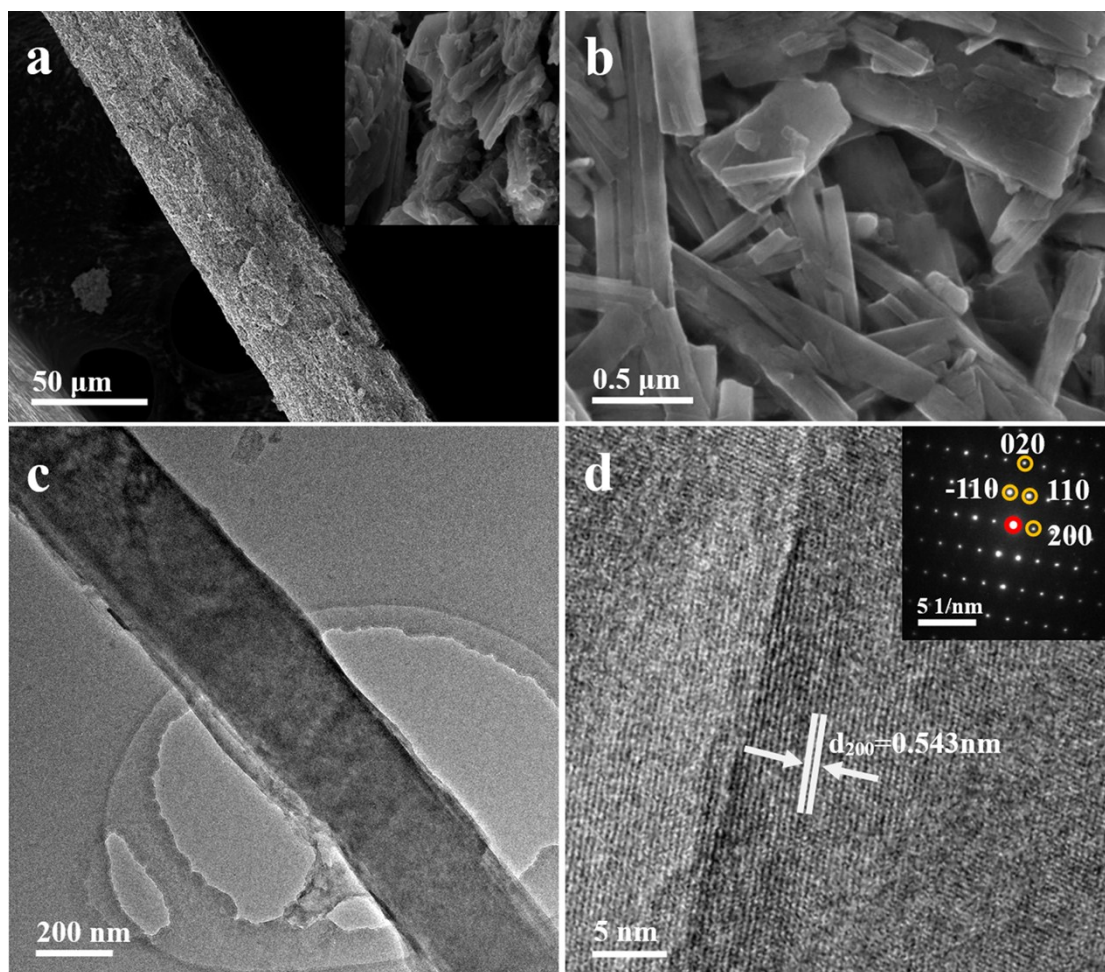


Figure S13 a) and b) SEM, TEM, and c) TEM images of the $(\text{NH}_4)_2\text{V}_{10}\text{O}_{25}\cdot 8\text{H}_2\text{O}$ electrodes obtained as discharged to 0.7 V in the initial cycle. We can see that the electrodes are composed of belt-like morphologies. d) A HRTEM image exhibits the (200) lattice fringes with a d-spacing of 0.543 nm, indicating that the phase has not changed in the fully discharge stage.

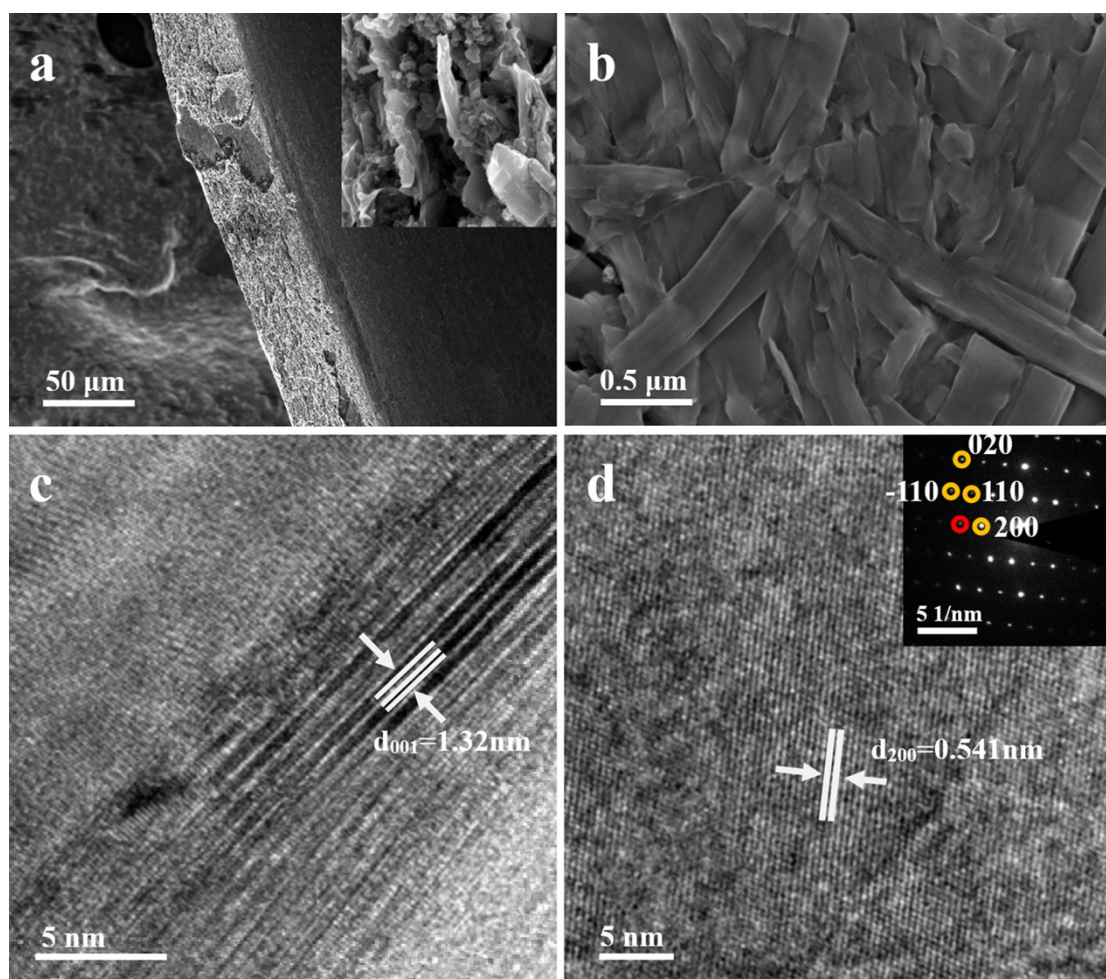


Figure S14 a) and b) SEM images of the $(\text{NH}_4)_2\text{V}_{10}\text{O}_{25}\cdot 8\text{H}_2\text{O}$ electrodes obtained as charged to 1.7 V in the initial cycle. We can see that the electrodes are composed of belt-like morphologies. c) HRTEM image presents a bilayer spacing of 1.32 nm that corresponds to the d_{001} spacing of $\text{V}_2\text{O}_5\cdot n\text{H}_2\text{O}$. While a HRTEM image (Figure s11. d)) exhibits the (200) lattice fringes with a d-spacing of 0.541 nm, indicating that the phase has not changed in the fully charge stage except a little expand in d_{001} spacing.

References

- 1 H. Ma, Sh. Zhang, W. Ji, Zh. Tao and J. Chen, *J. Am. Chem. Soc.*, 2008, **130**, 5361–5367.
- 2 D.M. Wei, H. Sugihara, I. Honma, M. Ichihara and H.S. Zhou, *Adv. Mater.*, 2005, **17**, 2964–2969.
- 3 D. Kundu, B.D. Adams, V. Duffort, S.H. Vajargah and L.F. Nazar, *Nat. Energy*, 2016, **1**, 16119.
- 4 C. Xia, J. Guo, Y. Lei, C. Zhao and H. N. Alshareef, *Adv. Mater.*, 2018, **5**, 1705580.
- 5 A. Moretti and S. Passerini, *Adv. Energy Mater.*, 2016, **6**, 1600868.
- 6 G.S. Gautam, P. Canepa, R. Malik, M. Liu, K. Persson and G. Ceder, *Chem. Commun.*, 2015, **51**, 13619–13622.